Erosional and Depositional Processes at the Lunar Surface

David Thorpe
Aberystwyth University
2021

THESIS
Submitted to Aberystwyth University
by
David Thorpe
In Candidature for the Degree of
Master of Philosophy
Supervisors: Tony Cook, Manuel Grande
Faculty of Business and Physical Sciences - Department of Physics

September 3, 2021

Abstract

Chandrayaan-1 X-ray Spectrometer high energy data were used to measure the width of the Earth's magnetotail comparing this measured value with measurements from a computational magnetohydrodynamic model, known as the Open Geospace General Circulation Model. The data from C1XS were taken from the high energy channels of the device, where a large spike in count rates represents an influx of energetic particles with energies above a few MeV, which become minimum ionising particles and deposit energy in the detectors at the 18-19 keV range. The C1XS data and OpenGGCM data agree on a magnetotail width of between $50R_E$ and $70R_E$ fluctuating with the strength of the solar wind. An analysis of the distribution of transient lunar phenomena was performed with the intention of studying two theories relating to the origins of TLP. The first theory is that TLP are caused by outgassing at the boundary between lunar highland and mare terrains. Previous studies have been conducted suggesting a correlation between TLP locations and these mare borders, but it was found in this analysis that this correlation does not appear in the most robust and reliable data and that this correlation can be created or removed depending upon the decision to classify the Aristarchus Plateau as a highland terrain. The second theory studied is the creation of TLP from the splitting of rocks on the lunar surface. It has previously been calculated that rocks splitting from thermal stresses or meteoric impacts could create a piezoelectric effect exciting gases released from the cracks and creating a flash visible from Earth. This analysis used a NASA database of lunar impact flashes to search for any clustering of reports that would be a signature of a localised environment susceptible to rock fracturing. The analysis found no evidence of any localised effects and an impact catalogue consistent with a randomly

distributed dataset, suggesting the proposed TLP explanation is either a rare occurrence or produces light obscured to an Earth observer.

Contents

1 Literature Review

This thesis is about erosional and depositional processes at the lunar surface. It covers the topics of high energy particles in the Earth's magnetosphere and using them to measure the magnetosphere, transient lunar phenomena and their correlation with the border between the two main lunar terrains, and a type of TLP known as the 'Zito effect' and whether their presence can been seen in a catalogue of similar flashes caused by meteoric impact. This chapter discusses the existing literature covering these topics and acts as an extended introduction for the topics to be discussed after.

1.1 C1XS - Chandrayaan-1 X-ray Spectrometer

The C1XS instrument is the successor to D-CIXS (Demonstration Compact Imaging X-ray Spectrometer) which was flown on-board the SMART-1 mission [1]. The primary aim of D-CIXS was to create global elemental abundance maps of the Moon, as discussed in '*The D-CIXS X-ray mapping spectrometer on SMART-1*' [2], being the first instrument to use x-ray fluorescence for this purpose. This new generation of X-ray spectrometers use swept charge devices (SCDs) [3] which have been likened to 1 dimensional X-ray CCDs, with faster read out and with a larger area [4].

C1XS flew onboard Chandrayaan-1, India's first mission to the Moon, which launched on the 22^{nd} October in 2008 [5]. The aims of Chandryaan-1 were to further our understanding of the evolution of the Moon. The spacecraft carried an array of instruments to do this including a terrain mapping camera (TMC), a hyper-spectral imager (HySI), a low energy X-ray spectrometer (C1XS), a high energy X-γ ray spectrometer (HEX) and a lunar laser ranging instrument (LLRI) [6] and an X-ray Solar Monitor (XSM) to measure the x-ray flux of the sun, against which lunar fluorescence can be calibrated [7]. C1XS was built in the Rutherford Appleton Laboratory (RAL) and supported by ESA [8].

Lunar X-ray fluorescence begins with irradiation by the Sun which produces a range of X-rays between 0.1 and 20 keV that are absorbed by the very top layer of the lunar surface, to a depth less than 200 μm. The Moon then fluoresces in X-rays at wavelengths characteristic of the elements fluorescing.

Results from the C1XS mission are discussed in 'The Chandrayaan-1 X-ray Spectrometer: First results' by Weider [8]. The paper focused on results from early within the mission's lifetime based on two A-class solar flare events in December '08 and January '09. The analysis in the paper did not use data from the XSM mounted to C1XS because the A-class flares were a magnitude weaker than the flares XSM was designed to characterise, and so the instrument could not reliably determine the input spectrum. They therefore used a modelled spectrum from AtomDB [9]. AtomDB is a database of atomic data and a plasma modeling code with a focus on X-ray astronomy, which generated a high-resolution modelled solar spectrum. Uncertainty existed over their ability to infer solar flare temperatures, which were estimated to be between 2.5 and 3.1 MK, based on the work of Kay *et al* [10]. To combat this they modelled C1XS spectra using both the upper and lower limits and factored it into their error reporting. The paper finds evidence for localised sodium detection of up to 1.65 ± 0.45 wt% but cannot say this is any more than tentative evidence as the signal could easily be mimicked by scattered solar flux if there is a high scattering efficiency.

The first unambiguous measurements of enhanced sodium on the lunar surface are reported by Athiray in 'C1XS results - First measurement of enhanced sodium on the lunar surface' [11]. Previous X-ray spectrometers on SMART-1 and Kaguya were damaged by radiation on their journey to the Moon, and so the data provided by them has been limited [12]. C1XS, in part to its shielding and part to it's travel occurring at solar minimum, survived the radiation much better and was able to record data for 9 months. This good fortune also has a downside, the low solar activity meant that there was not enough data to create global lunar maps of elemental abundance.

Athiray [11] uses two criteria in choosing which data to use: 1) identification of useful observations corresponding to solar flares, and 2) selection of good observation intervals where the observed data are not contaminated by any sudden increase in the flux of charged particles. This was done so that only the highest quality data will be analysed and the chances of detecting the presence of sodium will be increased; however, it meant that only a small portion of the lunar surface was analysed.

Athiray chose a B3 class flare as the threshold for good data (shown in figure 1), flares at lower classifications than this will not produce hard enough X-rays to reveal the higher energy Ca, Ti and Fe emission lines, resulting in highly unreliable abundance values post analysis. The algorithm used by Athiray to derive absolute elemental abundances was newly written by the author and has not been other-wise verified, however Athiray did run laboratory based XRF experiments on various metals and lunar analogous rocks to validate 'rigorously' as detailed in 'Experimental Validation of XRF Inversion Code for Chandrayaan-1' [13]. Athiray's analysis showed that the surface layer of the Moon contains much more sodium than had previously been detected. The results were >1 wt% Na, compared with <1 wt% from lunar samples, and reaching 5^{+0}_{-1} wt%

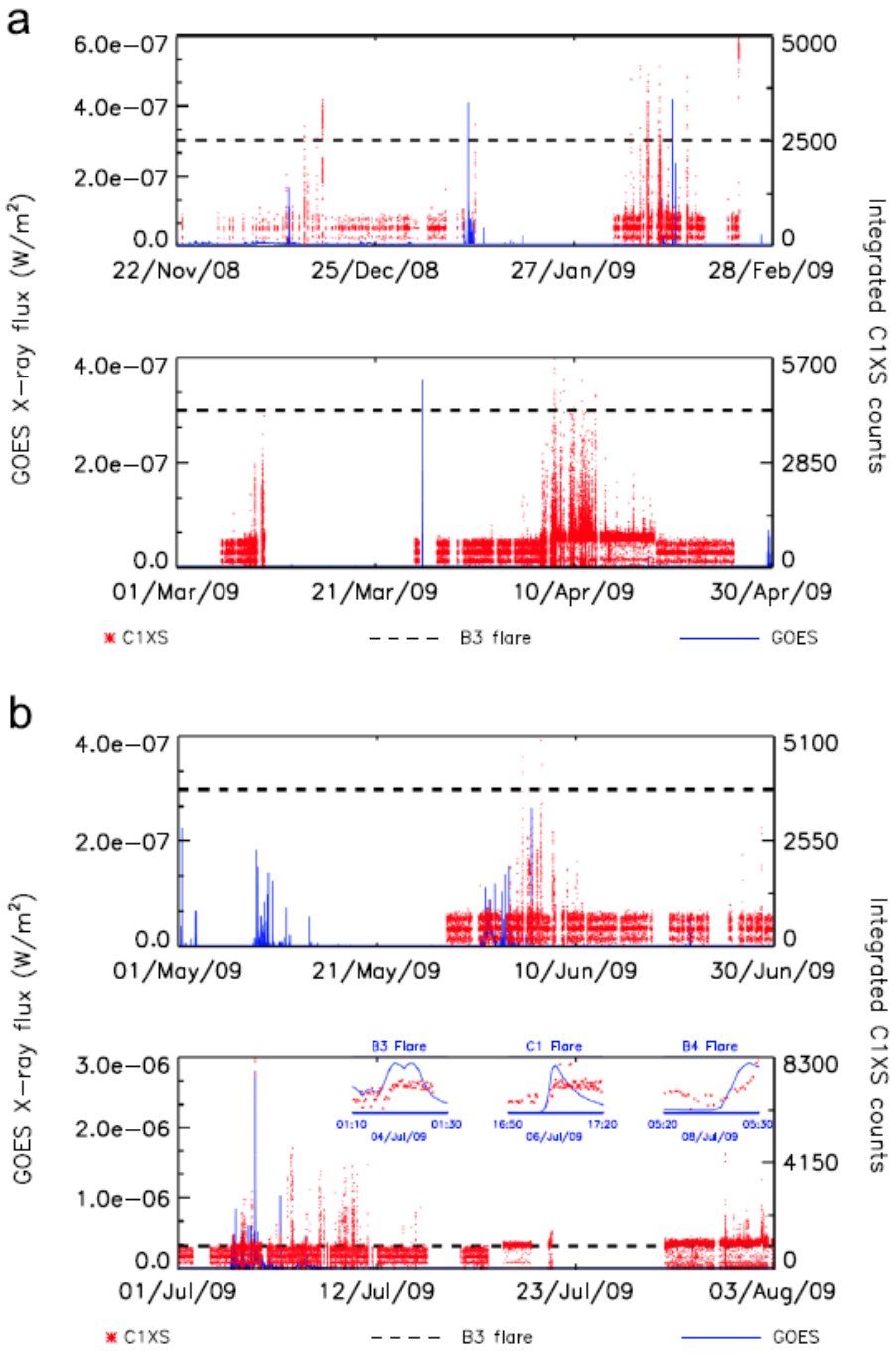

Figure 1: Full C1XS mission X-Ray flux. Red indicates C1XS integrated counts with 16 second bins. The blue lines indicate solar X-ray flux with time bin of 1 minute. The dashed line indicates the intensity of B3 class flares.

Although designed for detecting X-rays, Shyama Narendranath attempted to show that C1XS can also be used as a particle detector in her presentation 'Observations of the Geotail While in Lunar Orbit by the Chandrayaan-1 X-ray Spectrometer (C1XS)' [14]. During the transits by Chandrayaan-1 through the Earth's magnetotail, C1XS detected energy being deposited by energetic particles in the SCDs. Narendranath explained that these represent important measurements of deep tail width and dynamics. Narendranath presented a graph showing the total counts detected in 16s intervals over the whole duration of the mission in the high energy range 15-20 keV (figure 2). As the sun was quiet in X-rays during this time the counts are indicative of particle flux and it is claimed correlate well to ± 3 days of the full Moon, the period where the Moon and Chandrayaan-1 in lunar orbit are deepest within the Geotail. From the graph this is not immediately apparent as although the peaks in counts do coincide with full Moons, the width of these peaks appears to be multiple weeks, perhaps even a month in width depending on how the peaks are measured. The peaks in Narendranaths' graph are far from uniform in shape as well with two of the Geotail passes having an apparent double peak.

Narendranath has used the GEANT4 simulation toolkit [15] to study how charged particles would interact with the SCDs filter and collimators. Particles from a range of energies were modelled to determine at what energy the particles would deposit within the 1-20 keV range of detectors. It was found that particles beyond a few MeV become minimum ionising particles (MIPs) and deposit energy in the 18-19 keV range, allowing it to be used as a proxy for charged particle intensity measurements. This is demonstrated by a sharp increase in count rate at 18-19 keV in the C1XS data. With C1XS, converting the count rate into particle intensity is hampered by not

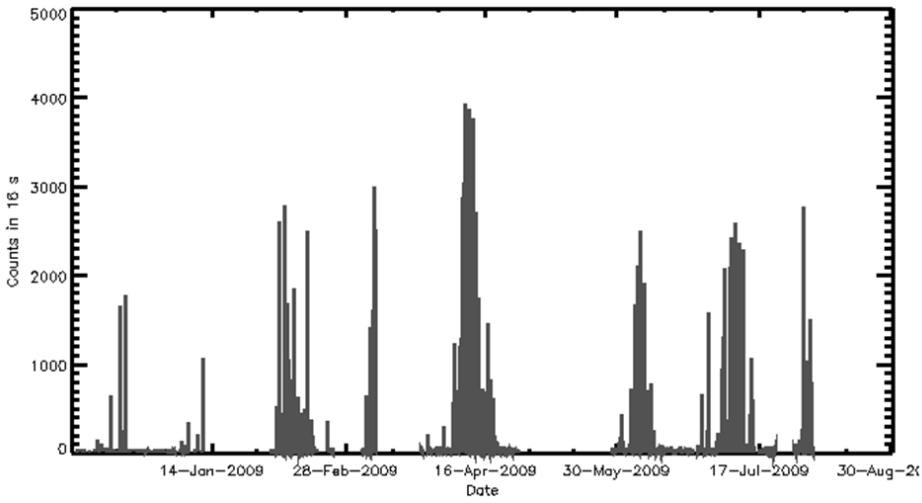

Figure 2: C1XS geotail passes, as presented by Narendranath in *Particles In the Lunar Environment: Observations of the Geotail While in Lunar Orbit by the Chandrayaan-1 X-ray Spectrometer (C1XS).*

having cross calibration data and having to rely on modelling, however a third generation of the C1XS detector, CLASS (Chandrayaan-2 Large Area Soft X-ray Spectrometer) [16], launched on-board Chandrayaan-2 [17] in July 2019 where the calibration problem may be rectified and simultaneous detections of X-ray and charged particle events will be possible. Narendranath's presentation to the 40th Lunar and Planetary Science Conference raised the important point that the Geotail can be studied using C1XS high energy data, something that was not part of the original science objectives of the mission.

1.2 Transient Lunar Phenomena

Transient Lunar Phenomena (TLP) are ephemeral changes in the appearance of the lunar surface. TLP come in 3 main categories as presented by Chilton: Glows, hazes and flashes [18]. Chilton did not put forward any theories of his own but took time to explain various other theories of TLP origin. Chilton regarded outgassing as the most likely source of TLP, released from gravitational disruptions to the Moon at perigee and apogee, causing the surface to crack. It was also posited that TLP activity may be related to solar activity with Chilton asserting that TLP usually occur just after outbreaks of sunspots, a theory that was proven wrong in 1966 by Burley and Middlehurst [19]. In his publication Chilton called for extra observers to look for the phenomena, as echoed in perhaps a more public domain by Clarke in the 'Astronomy Now' magazine (2001) [20]. While studying the phenomena would definitely be aided by more routine observations of the Moon, there is a danger that asking people to look for specific phenomena will lead to an increase in spurious reports that could potentially insert large bias into an analysis. This is further exacerbated in the article as Clarke tells the reader where the best places to look for TLP are, according to the number of reports, such as Aristarchus where 1/3 of all TLP reports originate. This could create an observational bias towards the mentioned features in future reports. Clarke discussed how William Herschel, an astronomer of great renown, observed three reddish points of light on the lunar surface which he incorrectly ascribed to volcanoes, one of which he claimed was erupting. TLP have been reported for hundreds of years and are not a modern curiosity.

Clarke's Astronomy Now article caters to the notion that TLP occur around mare edges, an idea that is popular with prominent TLP researcher Arlin Crotts. in the late '00s Crotts had three related papers published [21][22][23] discussing at length transient lunar phenomena. In his 2009 'paper 0', *Transient Lunar Phenomena: Regularity and Reality*, Crotts sorts the observation report data into samples by several parameters such as location of the observer or historical epoch, arguing that if the determining factor in reporting a TLP is one of these parameters, the TLP distributions of each samples will vary. Crotts found that this is not the case and concluded from this that the data is reliable and counts of spurious reports are low. The paper does not attempt to suggest a new process for TLP occurring, but rather discern whether TLP can be attributed to certain lunar features, perhaps narrowing down the list of possible causes. This is an important aspect of dealing with sporadic and ill-defined reports because, unlike a volcano on Earth, it is not possible to say that TLP, for example, occur directly over the central peaks of craters, it is therefore important to have an unbiased analysis confidently showing (or disproving) connections between features and phenomena. Crotts found that there are no statistical differences in observational biases except in an small interval between 1956 and 1968, in which a spike of reports focussed on Alphonsus, Gassendi and Ross D were spurred by previous reports. The reports analysed in paper 0 show 'a surprising amount of regularity' consistent with and suggesting that many reports are real. Crotts unusually concluded the paper 0 with assertions from his 2008 'paper 1' (*Lunar Outgassing, Transient Phenomena, and the Return to the Moon. I. Existing Data*), suggesting that TLP are connected to mare edges.

In paper 1 [22] Crotts used the data from his paper 0, which he has discerned as reliable and filters it for the most robust of the reports. Doing this will help the analysis' accuracy. As he wanted to see if there was a correlation with maria edges Crotts compared the distances of TLP report locations to maria edges with those of a random distribution, however, he uses a hand drawn boundary for the maria that happens to circle both the Aristarchus plateau and Plato crater. Being the two most numerous sites of his robust reports this border will massively skew the analysis result, and it is no surprise that he found TLP to be 7 times closer to the border than random points at 99.999% certainty. Paper 1 ends discussing mechanisms for TLP, devoting a whole chapter to outgassing.

The Moon has been shown to release small amounts of gasses, including argon and methane, leaving Crotts to ponder whether the source of gas release is endogenic or of meteoritic impact origin. Crotts showed a correlation between radon detection and the Aristarchus plateau suggesting radon release is related to the TLP observed here. He then showed a weaker correlation between weaker TLP sites and polonium enhancement, ^{210}Po being a daughter product of radon, both being tied to his hand drawn mare boundary. This he claimed is strong support for tying TLP to outgassing. The problem with this treatment is there is no direct link between the radon release and TLP being observed.

Toward the end of the paper Crotts revealed that deep moonquakes, at depths of 500 - 1,500 km, are also strongly correlated with mare edges. At this depth the deep moonquakes should have no association with mare basalt plains, as Crotts admits, but their correlation is stronger than that of the shallow moonquakes. Neither shallow nor deep moonquakes showed a close correlation in time with TLP report implying that in this scenario,

of quake induced TLP, large amounts of gas must be being released, as ^{222}R has a half life of three and a half days.

In the final of the three papers Crotts discussed how outgassing may develop into observable TLP [23]. The abstract of this paper poses an important question: 'TLPs betray some outgassing, but does outgassing necessarily produce TLPs?' This is important because the ideas implied in his previous papers suggest that outgassing and TLP are firmly linked, but because there is a small amount of gas release at the same sites as some TLP, this does not infer a relationship between them. The paper concludes the same. There is not evidence of enough radon production to produce the explosive outgassing that Crotts models in paper 2 required to create TLP like events. However, Crotts still enjoys the idea of outgassing and mentions that radon and polonium are good tracers for outgassing, even if not enough on their own to produce TLP, and that argon is a probable source, given that much of the Moon's tenuous atmosphere is composed of this [24]. Helium is also a major constituent of the Moon's atmosphere, but the source of this gas can easily be confused with that of solar wind origin. It is presumed that radon and argon both favour KREEP terrain, such as the western maria regions, suggesting that detections of these gasses and potentially, if linked TLP, are connected to the maria themselves.

1.3 Erosional and Depositional Processes

In 1972 Garlick was able to show that fluidisation of dust, occuring when vibrations cause a loss of intergrain cohesion [25], could account for the increase in brightness required to witness TLP against the bright lunar background from Earth. In the 1977 paper '*Lunar Surface Movements - the Evidence and the Causes*' Garlick discussed lunar seismic activity [26] presenting 3 types of activity. Deep quakes are unlikely to cause surface disturbances of dust because the quakes would not carry enough energy 800-1,000km to the lunar surface from their origin. Thermally induced quakes would be most prominent after lunar sunrise correlating with an increase in TLP reported by Cameron around sunrise [27]. The third seismic event is a shallow moonquake. These shallower moonquakes, although infrequent, would give larger wave amplitudes at the surface of the regolith, having the potential to disturb more dust and perhaps loose boulders on crater slopes. A lunar soil mechanics study, by Houston *et al* showed that such crater wall boulders are unlikely to be released unless the gradient of the slope is greater than 48° [29].

Lunar dust can be detrimental to human activities on the Moon due to its small size and sharp and angular surface. It can cause irritation of the eyes and throat [30] and it was also argued by Pendleton [31] in '*Dust Analysis at the Moon*' that the fine particles are a hazard to hardware and mechanical objects on the Moon. Dust can be levitated electrostatically on the Moon, due to solar UV ionisation, although this can only account for dust levitated several metres. To account for observations of dust grains at up to 100 km altitudes [32], Pendleton referred to Stubbs' work on '*The Dynamic fountain Model*' [33] in which he described narrow sheath regions

where dust can be accelerated rapidly and then lofted ballistically up to these heights. This model describes particles of up to 1 μm being lofted to 100km and reaching a maximum velocity on the same timescales (30s - 300s) as observations of Lunar Horizon Glow variations as described by McCoy. More recently the Lunar Dust Experiment (LDEX) aboard the LADEE mission (Lunar Atmosphere and Dust Environment Explorer) has observed a permanent dust cloud surrounding the Moon generated by surface impacts of interplanetary dust grains, but concluded that there was no indication of the dust populations required to produce the Lunar Horizon Glow [34]. Pendleton's publication also suggested some mission concepts that would help study the distribution of dust over the lunar surface including robotic orbiters and landers as well as 'astronaut deployable experiments'. These missions and new studies will be vital in assessing how to proceed with and how to minimise both risk and cost of future lunar exploration.

2 C1XS Magnetotail Measurements

2.1 Introduction

The Chandrayaan-1 X-Ray Spectrometer (C1XS) flew onboard Chandrayaan-1 lunar mission and captured data for 9 months in 2009. During this time the spacecraft transited the Earth's magnetotail whilst orbiting the Moon. This chapter discusses the usefulness of spectrometers as particle detectors in recording measurements of the Earth's magnetotail at lunar distances.

2.2 C1XS and X-Ray Spectrometry

An X-ray spectrometer can be used to determine the abundancies of specific elements within a surface, as each element will fluoresce with a characteristic wavelength when excited by solar radiation. To measure this, C1XS used an array of 24 SCDs behind a gold coated collimator (figure 3) allowing a spatial resolution of 25km, from Chandryaan-1's orbit altitude of 100km [7]. Lunar X-ray fluorescence is dependent upon incident solar soft X-ray radiation exciting the atoms and so C1XS was accompanied by an X-ray solar monitor (XSM) for calibration. During the time of Chandrayaan-1's mission the Sun was undergoing an extended minumum and the number of solar X-ray events was limited. For the few solar flares of soft X-ray energies that C1XS observed however, it was possible to create a partial abundance map for the Moon and for the first time detect the abundancies of sodium in the lunar surface [11].

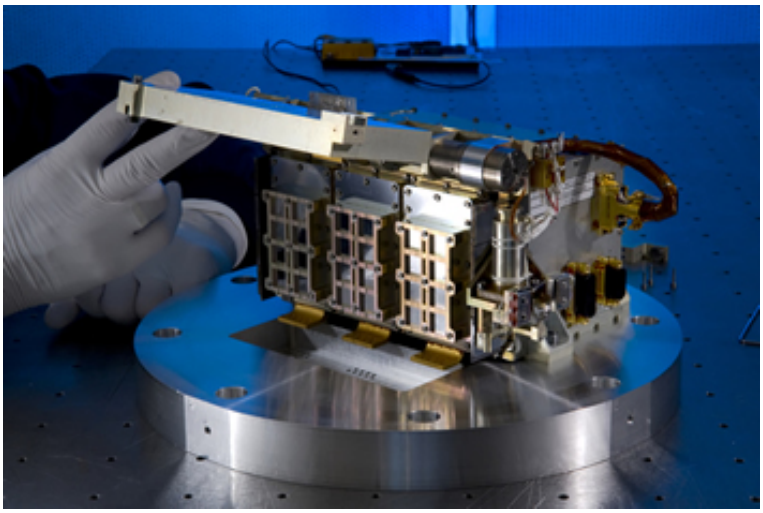

Figure 3: The C1XS instrument as displayed by RAL Space at *www.ralspace.stfc.ac.uk/Pages/Chandrayaan-1.aspx*

2.3 The Magnetotail

Earth's magnetotail (the Geotail)(figure 4) is a dynamic structure, varying in size with solar wind pressures and magnetic field orientation. The geotail forms a wake in the solar wind downstream from Earth where plasma densities are drastically lower than the plasma outside. The plasma within the geotail is of a different population to that of the inter-planetary medium, coming mostly from ion populations from Earth rather than solar wind ions from the Sun. These charged particles, within the Geotail, are more energetic than solar wind particles, having been accelerated along the Earth's magnetic field lines and from magnetic reconnection within the tail. When looking at magnetic field strengths the magnetopause is clearly visible as a boundary between the Earth's magnetic field and the interplanetary magnetic field (IMF) [35].

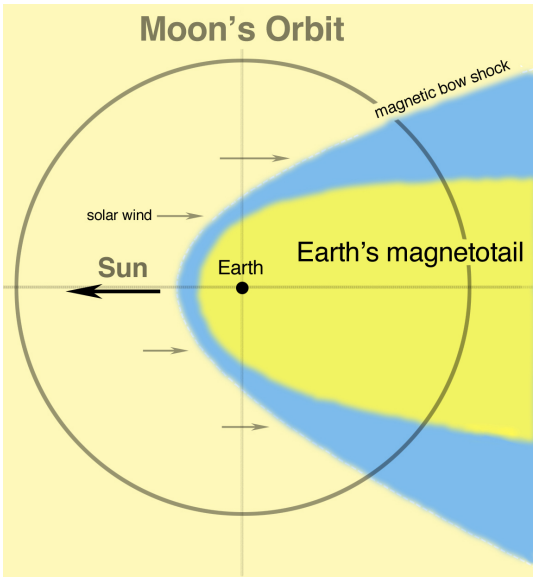

Figure 4: The Geotail as displayed by NASA at *www.nasa.gov/topics/moonmars/features/magnetotail_080416.html* by TJ Stubbs

2.4 Magnetospheric Model

The high energy data from C1XS can be checked against a simulated model of the Geotail to verify that C1XS is detecting the magnetotail via high energy particle interactions as described in chapter 1.1. For this purpose the Open Geospace General Circulation Model (OpenGGCM) was chosen. OpenGGCM is a magnetohydrodynamic (MHD) model of Earth's magnetosphere, created by Joachim Raeder at UCLA [36]. The model is run through The Community Coordinated Modelling Centre's (CCMC) 'runs on request' feature, situated at NASA Goddard Spaceflight Centre (GSFC), using ACE real time historical data for the solar wind input. OpenGGCM allows for the simulation of the magnetosphere several hundreds of Earth radii downstream of the Earth and suitable for the $X = 60R_E$ orbit of the Moon. All CCMC run results are posted on their website for public viewing and return data and visualisation tools depending on the simulation model chosen. With OpenGGCM, CCMC provides 2D cross-sections of the magnetosphere in user defined planes for a variety of outputs including magnetic field strengths B_x, B_y, B_z, particle densities and plasma pressures.

2.5 Analysis

C1XS count rates are reported for each 16 second interval of the mission. Using the high energy channels from C1XS (18-19 keV) as reported by Narendranath [14] it is clear that the MIP energy deposits rise dramatically once each month around the Full Moon (Figure 2). At the time of a Full Moon the Moon, and Chandryaan-1 and C1XS with it, are directly behind the Earth in the X-Y plane and passing through the geotail at $\sim 60R_E$.These spikes in the count rate begin roughly 3 days before and end 3 days after the maxima, suggesting a 6 day transit time through the geotail.

The simulated output from OpenGGCM is used for viewing different structures within the magnetotail. Particle density is a very good descriptor of the bow shock and magnetosheath, where large numbers of solar wind particles are compressed against the subsonic plasma surrounding the Earth's magnetic field. At lunar distances however, the inner boundary of the magnetosheath, as seen by particle density, is fairly diffuse making it hard to determine the edge of the magnetosphere, as shown in figure 5. The boundary of the magnetotail, the magnetopause, is more easily discernible in the magnetic field outputs B_x and B_z (figures 6 and 7) as the magnetic field strength across the magnetopause increases rapidly in the X direction and decreases equally as rapidly from the magnetosheath magnitudes in the Z direction. These steep gradients in magnetic field strength should make it possible to predict where in the C1XS data we can expect to see the high energy particle peaks begin, and end, for each transit.

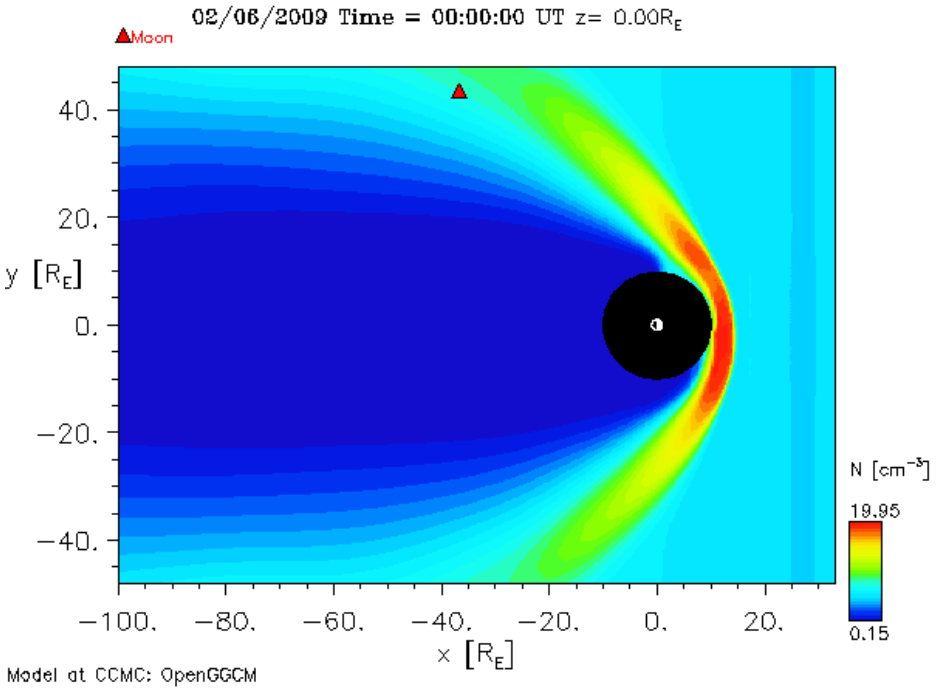

Figure 5: Numerical simulation of particle densities around Earth in the x-y plane. Earth is represented by the white circle at X,Y=0,0 with sunward side shaded white towards positive X. The Moon is represented by the red triangle and orbits at an average distance of 60 Earth Radii. The black disc around Earth is a mask used to prevent saturation of the colour bands. The magnetopause lies immediately behind the magnetosheath seen here in yellow and red, but at distances more than 10 Earth radii the gradient of particle density becomes too low to accurately identify this location.

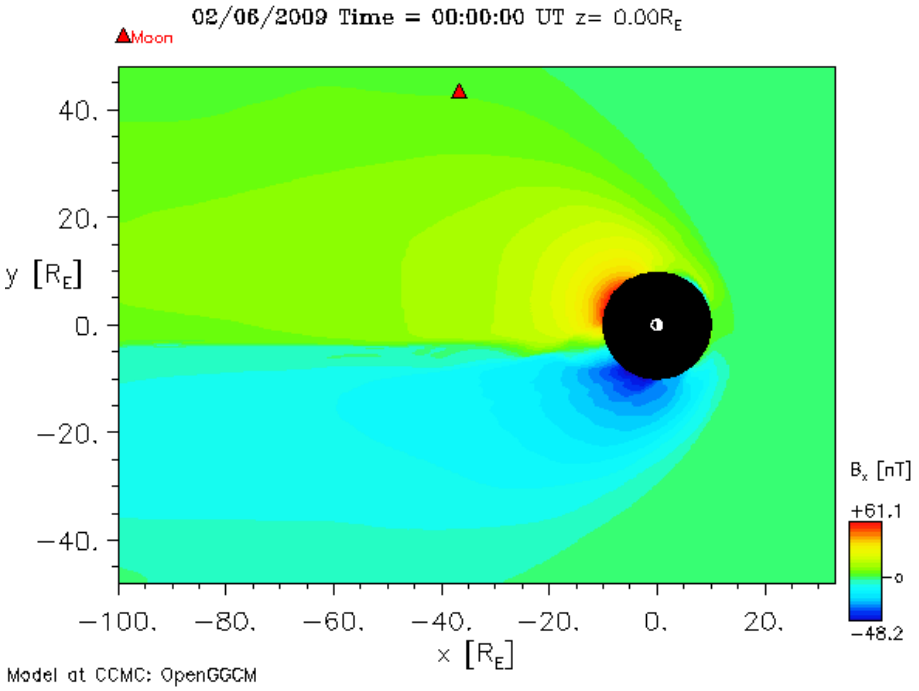

Figure 6: Numerical simulation of magnetic field strength along the Sun-Earth axis in the x-y plane, showing the B_x component of the magnetic field. Earth is represented by the white circle at X,Y=0,0 with sunward side shaded white towards positive X. The Moon is represented by the red triangle and orbits at an average distance of 60 Earth Radii. The black disc around Earth is a mask used to prevent saturation of the colour bands. The magnetopause here is visible at the transition from the green colour of the solar wind magnetic field to the blue and yellow colours of Earth's magnetic field, representing a change in direction of the magnetic field at the magnetopause.

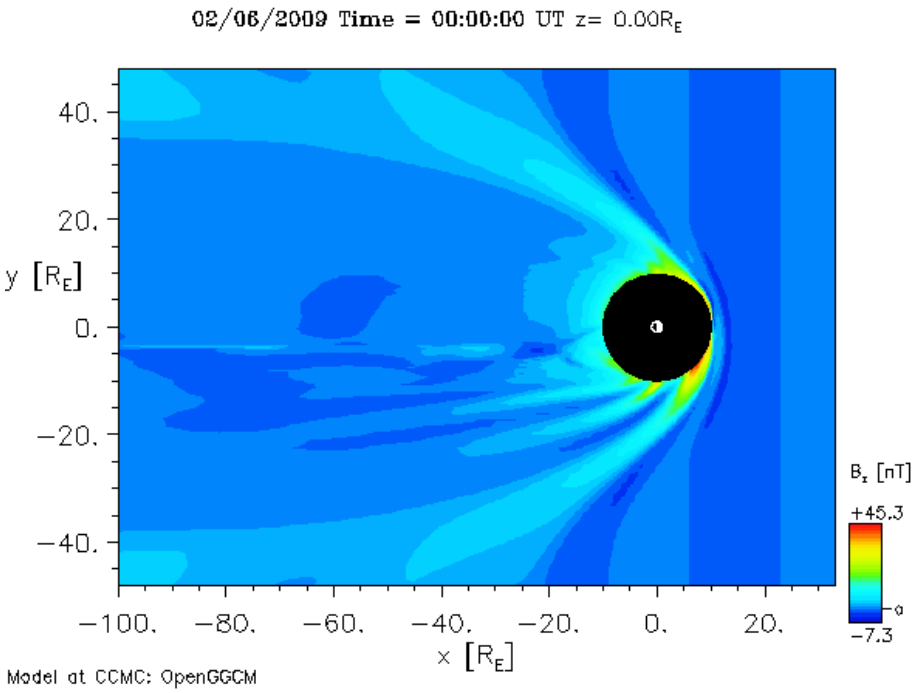

Figure 7: Numerical simulation of magnetic field strength along the north-south ecliptic axis in the x-y plane, showing the B_z component of the magnetic field. Earth is represented by the white circle at X,Y=0,0 with sunward side shaded white towards positive X. The Moon is represented by the red triangle and orbits at an average distance of 60 Earth Radii. The black disc around Earth is a mask used to prevent saturation of the colour bands. The magnetopause is visible as a sharp increase in strength of the B_z component of the magnetic field.

The Moon does not orbit in the Sun-Earth plane but at an inclination of 5.14°. This will lead to variation within the position of the Moon with respect to the magnetopause each transit. This inclination leads to a maximum height above or below the ecliptic of $Z = \pm 5R_E$ (figures 6 and 7). It can be seen from the simulations shown in figures 8 and 9 that this difference corresponds to little variation in the plasma parameters, and due to the imprecision in determining the time of C1XS's transition through the magnetopause this small variation can be ignored.

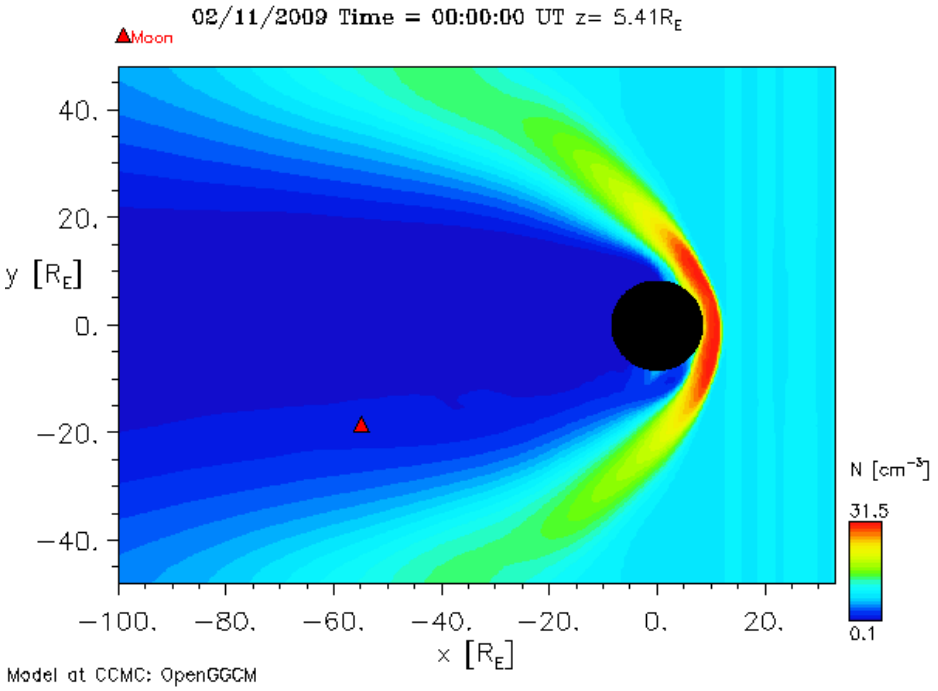

Figure 8: Numerical simulation of particle densities around Earth at a height of $5R_E$ above the ecliptic.Earth is represented by the white circle at X,Y=0,0 with sunward side shaded white towards positive X. The Moon is represented by the red triangle and orbits at an average distance of 60 Earth Radii. The black disc around Earth is a mask used to prevent saturation of the colour bands.

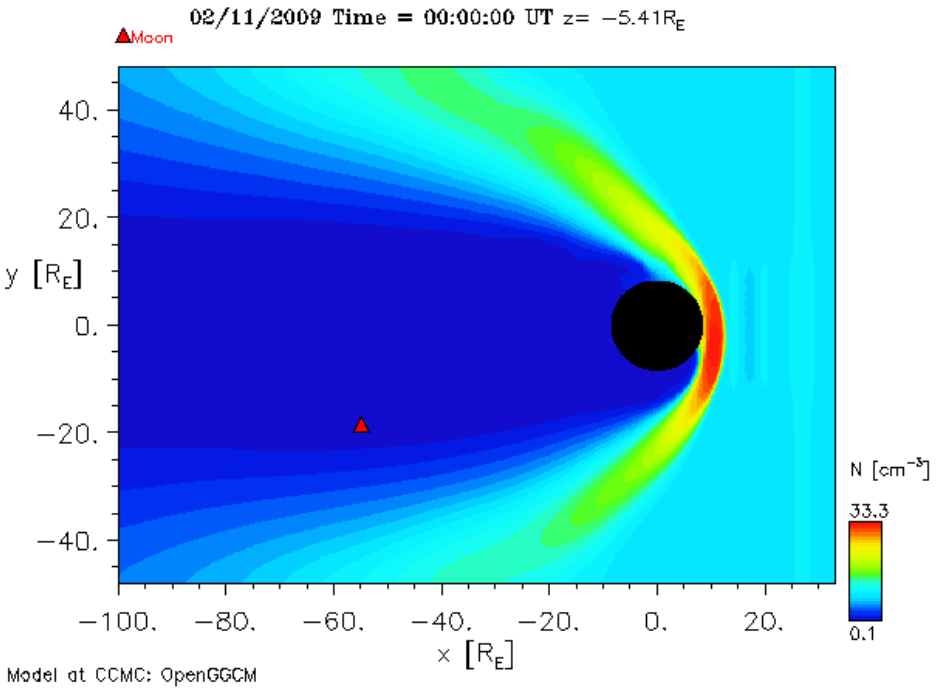

Figure 9: Numerical simulation of particle densities around Earth at a height of $5R_E$ below the ecliptic.Earth is represented by the white circle at X,Y=0,0 with sunward side shaded white towards positive X. The Moon is represented by the red triangle and orbits at an average distance of 60 Earth Radii. The black disc around Earth is a mask used to prevent saturation of the colour bands.

Data from OpenGGCM simulations (figure 10) show that strength of the B_z component of the mangetic field presents a transition window on the order of hours, and that particle densities present clear 'inside' and 'outside' regions of the magnetotail, but the transition window from this data is on the order of days.

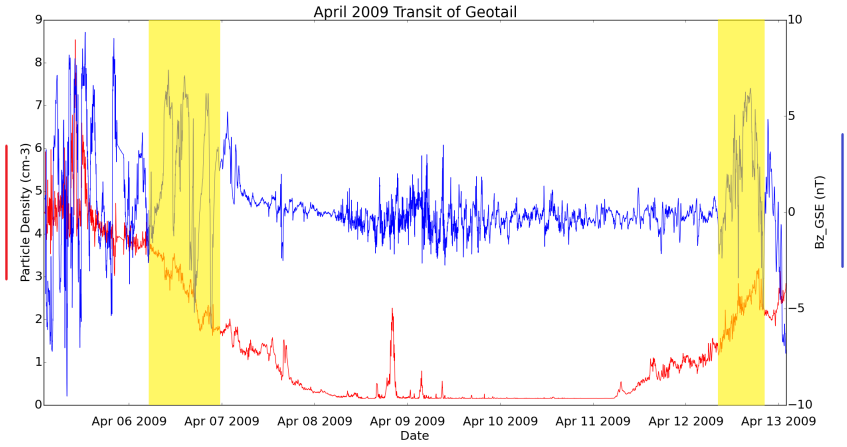

Figure 10: One dimensional time series comparing particle density and magnetic field z component at the Moon over April 2009. Magnetopause transits can be seen during the evenings of the 6th and 12th April as highlighted in yellow.

The simulated tail crossing for April 2009's transit matches the hourly count rates derived from the C1XS high energy data (figure 11), beginning on the 7th April and exiting the tail on the 12th April. This confirms the 6 day transit time and a magnetotail stretching $Y = 70R_E$ at lunar distances. This shows a magnetotail at $X = 60R_E$ as large as the maximum extent observed by the ARTEMIS (the Acceleration, Recconection, Turbulence and Electrodynamics of The Moon's Interaction with the Sun) mission [37].

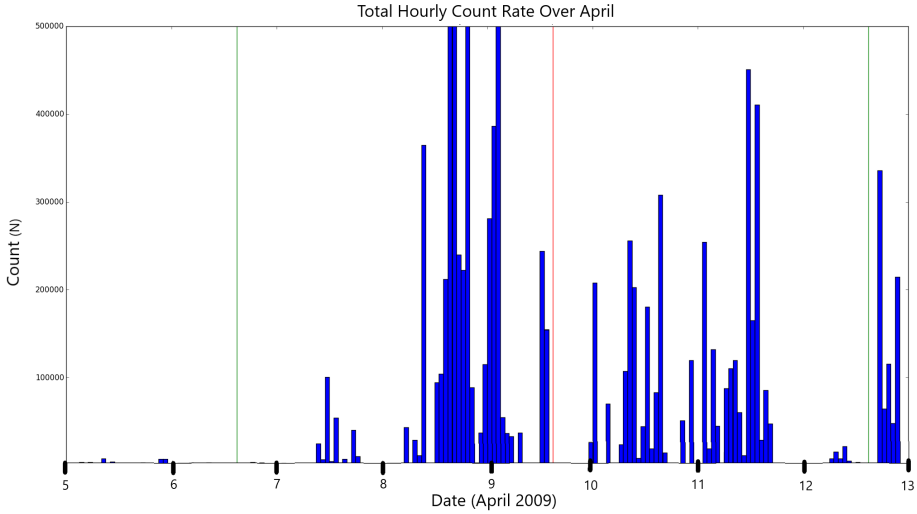

Figure 11: C1XS high energy data showing the hourly count rate for Chandrayaan-1's April transit of the Geotail. The detections begin during the 7th and last until the 12th. The time of the Full Moon is marked as a red line, with +/- 3 days of the Full Moon marked with green lines.

Other months, for which the C1XS data are not as as numerous and well defined as April, do not have such an unambiguous correlation. February has a very close match, being a direct mapping for the entry into the geotail but the simulation outputs do not give a very solid exit date which is also backed up by the C1XS data. July's transit exit simulation is the only magnetosheath crossing that is very poorly aligned with the real data (figures 12 and 13) and this may be explained by the turbulent extent of the magnetosheath, which varied rapidly over this transit period causing inconsistent particle detections in C1XS and a simulated plasma density reaching 40 cm^{-3} before fluctuating between 2 and 10 cm^{-3}. The C1XS data for March has significant coverage only of C1XS's entry into the magnetotail and not its exit, and the simulation and data are in agreement.

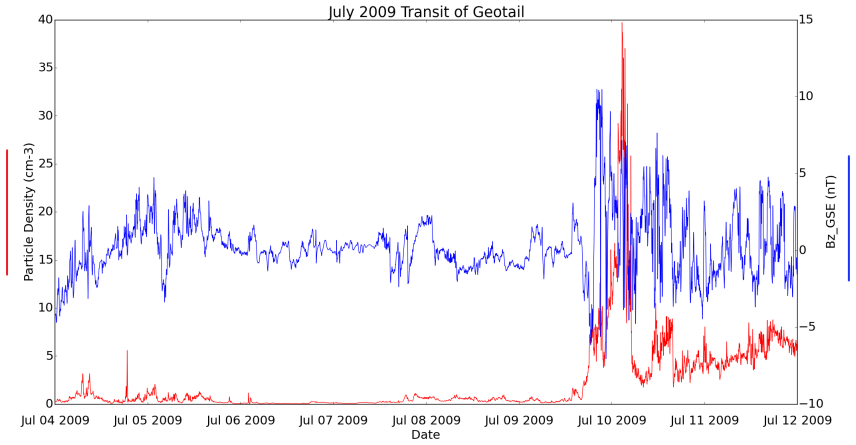

Figure 12: One dimensional time series comparing particle density and magnetic field z component at the Moon over July 2009. Chandrayaan-1 exits the Geotail on the 10th July in this simulation.

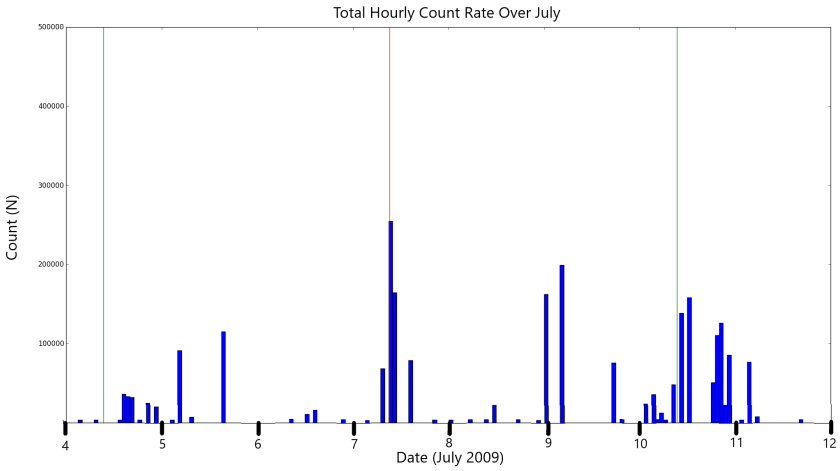

Figure 13: C1XS high energy data showing the hourly count rate for Chandrayaan-1's July transit of the Geotail. The time of the Full Moon is marked as a red line, with +/- 3 days of the Full Moon marked with green lines. C1XS was still detecting particles over the 10th and into the 11th of July after the simulation suggests it has left the Geotail.

The data received from C1XS could not provide a high resolution measurement of the magnetotail (about 24 hours) but is similar in resolution to predicted particle densities of the OpenGGCM model.

2.6 Conclusion

OpenGGCM has been used via CCMC to predict magnetotail transits through magnetopause crossings for the Moon and by proxy Chandryaan-1 in orbit around the Moon. This has then been compared to high energy (18-19 keV) detections in C1XS, corresponding to MIPs of electron and proton interactions in the C1XS detectors, confirming that X-ray detectors such as those in C1XS can be used as particle detectors to measure the extent of the magnetotail. Using C1XS data the magnetotail has been found to vary quite largely in size from $Y = 50R_E$ to $Y = 70R_E$ in diameter, as measured from time taken to transit it. The investigation also confirms the accuracy of the model at ranges up to $X = 70R_E$ when using historical solar wind data.

3 Transient Lunar Phenomena and the Mare-Highland Borders

3.1 Introduction

Transient Lunar Phenomena have been reported in many different forms from red glows to quick flashes of light and with equally varying explanations from outgassing to electrical discharges. Arlin Crotts put forward a series of influential papers purporting to show a link between transient phenomena and the borders between highland terrain and mare terrain [21][22][23]. This idea lent weight to the theory that outgassing was responsible for a sizeable portion of TLP as the mare could act as caps on a fractured highland terrain that would allow the gasses to percolate up to the surface and emerge at these boundary points. This chapter suggests that this correlation does not exist and that the link has been exaggerated by Crotts' definition of the Aristarchus Plateau as highland terrain.

3.2 Lunar Observations

The Moon is the closest celestial body to Earth and has been looked upon by humans for thousands of years. It was not until the invention of the telescope though, that humans have been able to accurately detail the Moon. On the 19th April 1787 renowned astronomer William Herschel reported seeing three red 'volcanoes' on the Moon [38]. However, it is believed that no volcanic activity has occurred on the Moon for 50 million years [39] and thus volcanism is unlikely to be the cause of his glowing red spots. Herschel is not the only astronomer to have noticed strange transient features on the Moon since the invention of the telescope, Halley, Olbers, Moore and Tombaugh are all respected astronomers with catalogued reports of transient lunar phenomena (TLP) alongside over 1,000 other reports [40].

TLP have been reported with many different visual characteristics, but can broadly be described as glows, such as Herschel's volcanoes, flashes, and clouds such as the lunar horizon glow [41] witnessed by Apollo astronauts and the Russian Lunokhod spacecraft. TLP can also have a colour attributed to them, with many reports being of a reddish colour.

3.3 Possible Sources

There have been many proposed explanation for TLP. Most of the reports of TLP come from amateur astronomers and are not verified by multiple witnesses leading to the possibility of mistakes. These include chromatic aberration, which can cause the red and blue light to refract separately in a lens and create the impression of colours on the lunar surface, passing satellites which can create a bright flash as they rotate and momentarily reflect the sun's light at the observer, or effects as described by Holden of

'favourable illumination of mountain ridges' [42].

Not all reports can be so easily explained though, having come from respected and experienced astronomers or having been witnessed by multiple sources. These include the Lunar Horizon Glow (figure 14), which is occasionally visible on the lunar horizon before sunrise, but extends beyond the usual zodiacal light. Stubbs has tried to explain this phenomenon using calculations of electrostatic dust lofting, raising charged dust grains up to 100km above the lunar surface[43], although more recent data from LDEX has suggested this model is inaccurate [44].

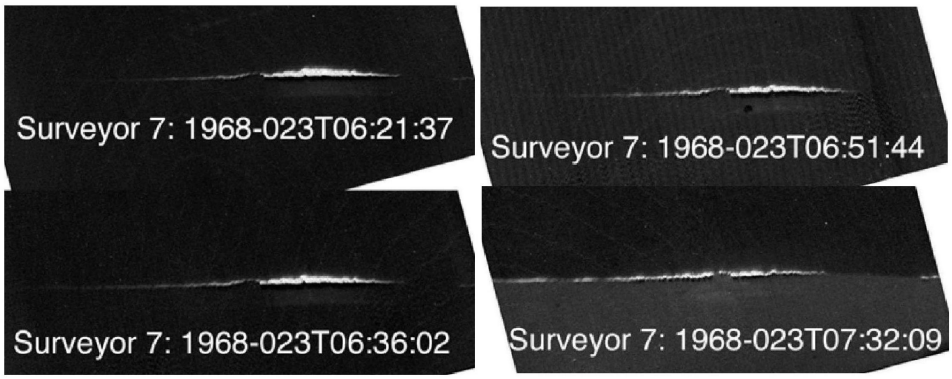

Figure 14: Lunar horizon glow as observed by Surveyor 7, displayed by NASA at *www.nasa.gov/centers/goddard/news/features/2010/lhg.html*.

Crotts suggested that many TLP occur due to outgassing from below the lunar surface and correlates TLP locations to the boundary between mare terrain and highland terrain [22]. This suggestion is flawed, and the correlation between TLP locations and the mare boundaries arises from the generation of Crotts' border, which he deduced by eye with a hand drawn curve. This chapter shows that Crotts' result is heavily influenced by his decision to include small boundaries around the craters Plato and especially Aristarchus, which alone accounts for more than 30% of all TLP reports.

3.4 Analysis

An unpublished catalogue of TLP reports compiled by Cook with over 2,000 entries is used in this analysis, with permission from the author. Cook has weighted the reports into 6 weight categories, 0-5, where category 5 are confirmed and unambiguous sightings with documented evidence, category 4 are reports confirmed by more than one observer, category 3 are observations from experienced observers, category 2 are reports Cook thinks are good but from inexperienced observers, category 1 reports are unlikely to be TLP, and category 0 are observational nulls which are reports of normal lunar appearance.

TLP sightings are not evenly distributed across the Moon's surface. The Aristarchus plateau accounts for approximately 30% of reports and Plato approximately 8%, features with diameters of 200km and 100km repectively. It is therefore important to analyse the data both with and without Aristarchus reports included.

If TLP are caused by an effect from a particular type or types of feature then it is expected that the reports should be grouped around said

features. For Crott's theory of explosive outgassing [23] to be a source of TLP, a correlation between mare-highland boundaries and TLP sightings must be drawn. Whereas Crotts hand drew this boundary and included the Aristarchus plateau, a decision that would heavily influence the result, for this study a Python code was written to analyse an image of the Moon and use the brightness difference between the dark mare terrain and the lighter highland terrain to create a border around the maria (figure 9). This provides a numerical way to determine how close a feature with a reported TLP is from the boundary. The resulting border has a more intricate shape than Crott's smoothed border but contains all of the same regions within it but differs from Crott's border as the Aristarchus Plateau is not marked out as highland terrain in the computer generated border.

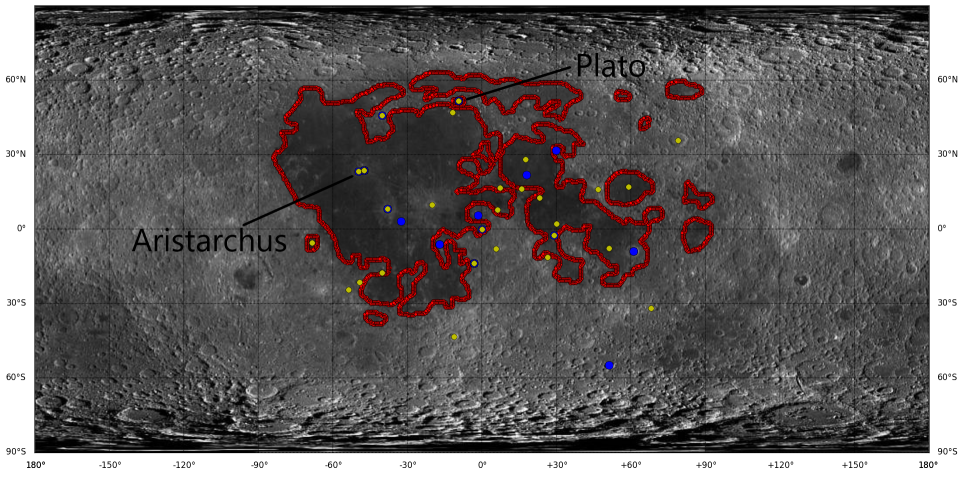

Figure 15: Visualisation of the numerically generated mare borders above a map of the Moon. The generated border data are shown in red, weight 4 TLP reports are represented by blue circles and weight 5 TLP data by yellow circles. With this border Aristarchus is clearly within the large mare of Oceanus Procellarum.

Measuring the distances of the coordinates of features of reported TLP events, without data from Aristarchus, to the closest generated mare border coordinate along great circle lines determines that there is very limited correlation with this border. The weights of data from 4 to 0 all show the most likely distance a report lies from the border is 50km or less. The strongest weighted and most reliable reports of TLP actually show that without counting the Aristarchus Plateau as highland terrain the most likely distance from a mare border for TLP to be is 50-100km (figure 16). When data from the Aristarchus region is used, still without counting the region as highland terrain, a large spike in all datasets (figure 17) is visible at 350-400km reflecting the over-abundance of reports at this location.

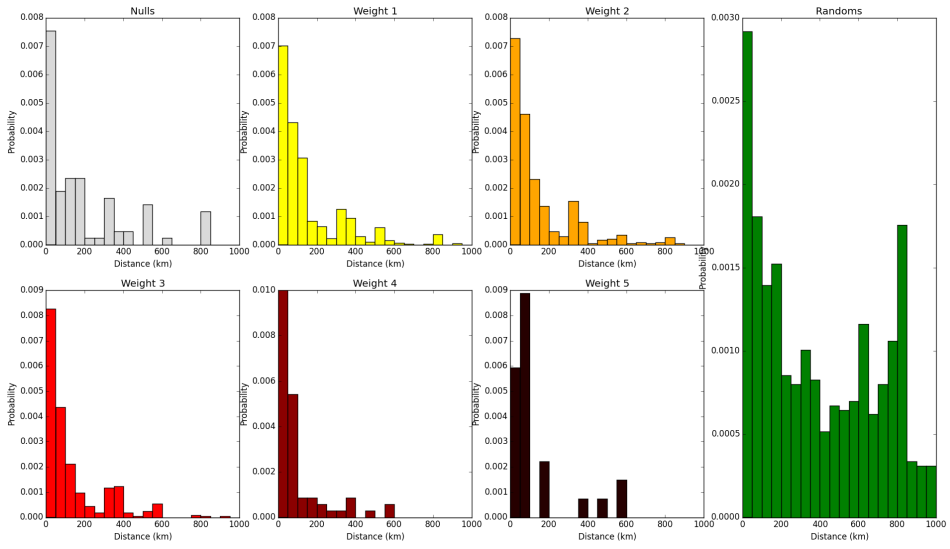

Figure 16: Histograms of minimum distance to the generated border for TLPs, except for those at Aristarchus, alongside a set of randomly generated events.

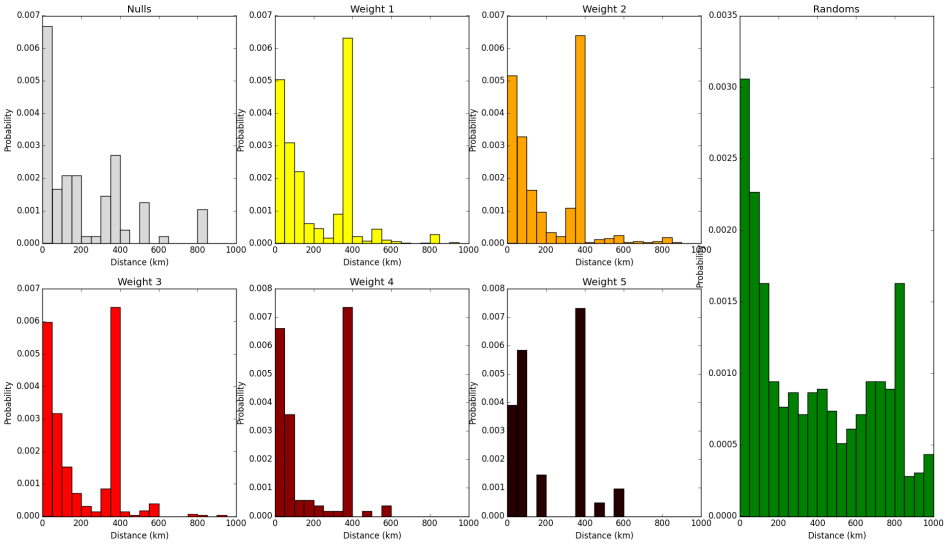

Figure 17: Histograms of minimum distance to the generated border for all TLPs, including data from Aristarchus reports, alongside a set of randomly generated events. The effect of the large amount of data from Aristarchus is present here at the 350-400km distance.

3.5 Conclusion

The data from lower weight and reliability TLP reports do suggest a correlation between maria boundaires and TLP events, however when the most reliable data from the weight 5 category (unambigous events with recorded evidence) are used the results differ from what is expected as shown by the randomly generated events. The weight 5 events are most often reported between 50 and 100 kilometres from any mare-highland terrain boundary. The idea supported by Crotts, that TLP occur around the borders between mare and highland terrain, only holds up when a border is drawn around the Aristarchus Plateau, and with such a high percentage of TLP reports being reported at Aristarchus an analysis with any border will be saturated at the point of closest distance between Aristarchus and this border. This

effect is clearly visible in figure 17 between Aristarchus and a border 350-400km away. Future discussion should therefore focus on the eligibility of treatment of the Aristarchus Plateau as highland terrain rather than part of the maria and whether the same underlying physical processes expected to occur at mare-highland borders, such as gas travelling around the mare basalts through cracked highland terrain, can be expected to occur at this location.

4 Constraining the Zito Effect

4.1 Introduction

The Zito effect was first proposed by Richard R Zito in 1989 [45] as a possible explanation for some transient lunar phenomena. Rocks splitting on the lunar surface due to thermal or seismic stresses or from meteoritic impact may produce light visible from Earth. This light would appear similar to meteorite impact flash such as those recorded by the Marshall Space Flight Center at NASA [46]. It is shown that the expected signals for such a Zito effect do not exist within the impact flash catalogue which is important to NASA's space mission meteor threat evaluations.

4.2 Transient Lunar Phenomena

Observers of the Moon have for centuries described transient phenomena [19] with descriptions of red volcanoes, hazy clouds, glowing blue lights and bright flashes. Richard Zito proposed an explanation for some bright flash TLP in 1989 [45]. He suggested that rock fracturing on the surface of the Moon, by seismic activity or by thermal stressing, can create a piezoelectric effect and release electrons that will excite gases contained within the rock that are also released by the fracture. His calculations showed that for basaltic rock with a density of 3.0×10^3 kgm^{-3} and a porosity of 10% a 1m crack penetrating to a depth of 8.5m would produce sufficient energy ($1\ W/m^2$) to create a flash visible from Earth through a small aperture telescope, at 8% brighter than the average lunar surface.

4.3 Impact Flashes

Lunar impact flashes are a well known phenomena. NASA's Marshall Space Flight Center has kept a catalogue of such flashes since 2006 [47] and they use this data to estimate danger to satellites because the Moon offers a much larger collection area for meteorites than can be achieved looking into the Earth's sky for meteors. Impact flashes are short in duration, being measured by NASA in 1/30ths of a second, (similar to the proposed Zito effect) and possible contamination of catalogue entries with Zito effect TLPs may over-represent meteorite impacts and thereby overestimate the danger of space missions. Nasa's catalogue of impact flashes is controlled to remove impact flash like effects, such as reflections and glints from satellites and point meteors ablating in Earth's atmosphere but effects such as the one described by Zito, that originate on the lunar surface, may not be screened out.

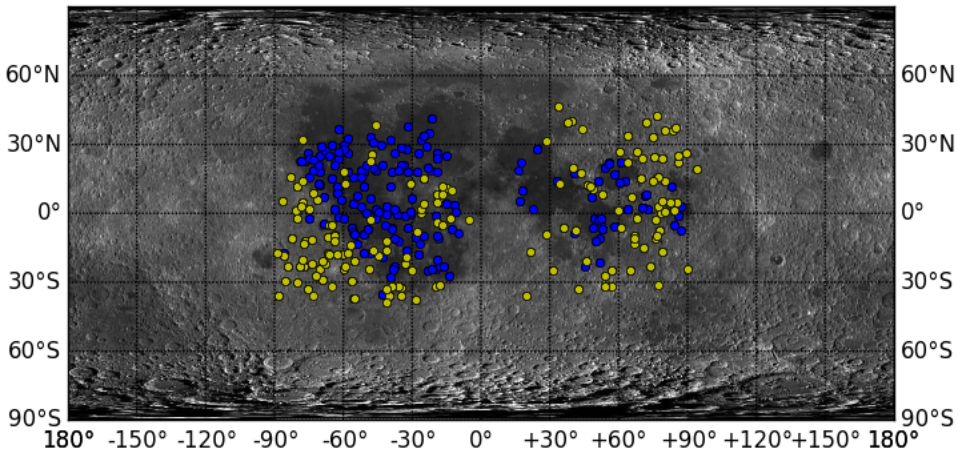

Figure 18: Locations of Marshall Space Flight Center catalogued impact flashes on the lunar surface. Impacts are coloured according to the terrain they landed on, with blue circles representing impacts landing on dark terrain, typically in the lunar maria, and yellow circles representing the impacts that landed on bright terrain, typical of the highlands.

4.4 Impact Flash Catalogue

The distribution of impact flashes across the lunar surface should be evenly distributed, with the western hemisphere having about 30% more impacts than the eastern hemisphere due to the leading edge effect, and the equatorial regions having about 10% more impacts than the poles due to meteoroids in the plane of the solar system. The actual distribution however, possibly due to observational effects [48] (shown in figure 18), has no impacts observed outside ±60 degrees, a marked drop in observations at the central longitudes and a much decreased number of observations in the eastern hemisphere. This is due to optimal observation scenarios, as observers will want to view the largest possible area of Moon unlit by the sun and so will avoid the poles as the crescent shape of the Moon's illumination ensures proximity to sunlight in those regions and the eastern hemisphere is best viewed at early hours of the morning when fewer observers are inclined to be active.

4.5 Analysis

For this analysis a random distribution of coordinates were generated to simulate an impact flash catalogue without any localised TLP intrusions. To ensure this closely matched the Marshall catalogue the same constraints as were predicted for the real data were applied: The data were generated with a sinusoidal longitude and latitude distribution to ensure lower reports at the limbs and at central longitudes and with a higher probability over dark backgrounds to reflect that it is easier to observe a flash with a larger brightness compared with its background.

The Marshall Space Flight Center impact flash catalogue matches well with the random distribution of coordinates as shown in figures 19 and 20. One pair of catalogued impacts were within 3km of each other, but the probability distribution of both randomised data and catalogued impact flashes suggest this is not too improbable at 0.2% probability for any pair of points in the distributions containing 330 reports.

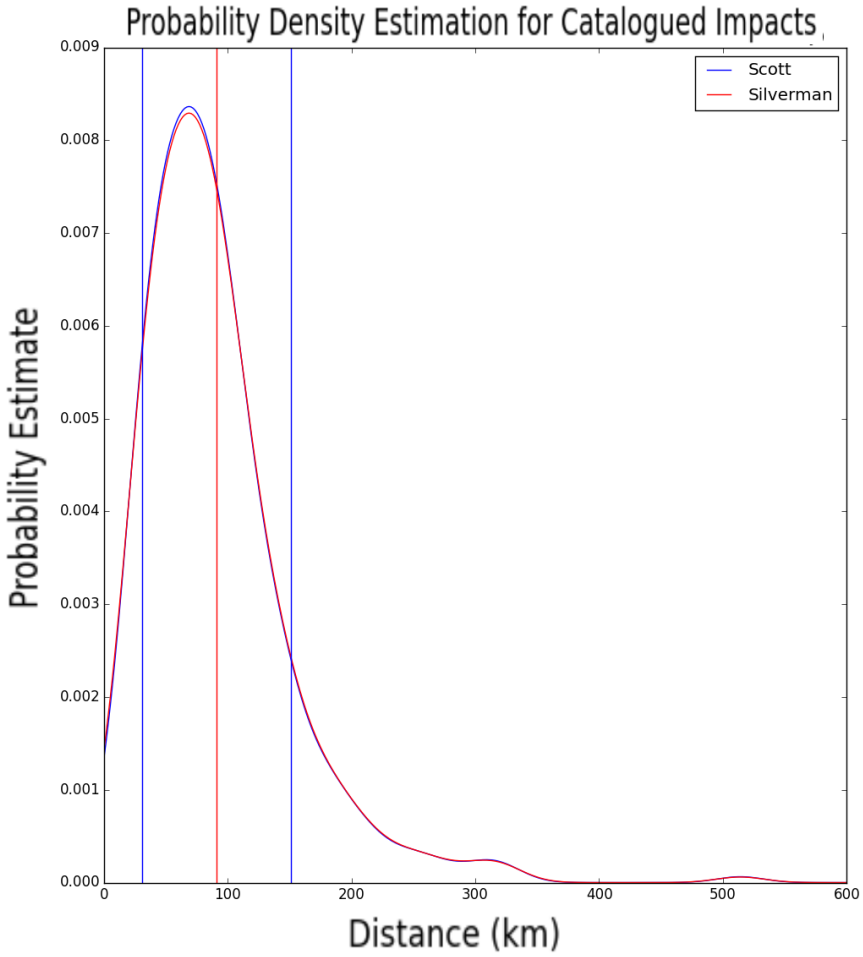

Figure 19: Probability estimates for the distance between any two observed impact flashes in the Marshall Space Flight Center catalogue. Mean separation is shown as the red vertical line and the standard deviation is shown as the blue vertical lines. Probabilities calculated using both the Scott and Silverman smoothing estimations are shown [49].

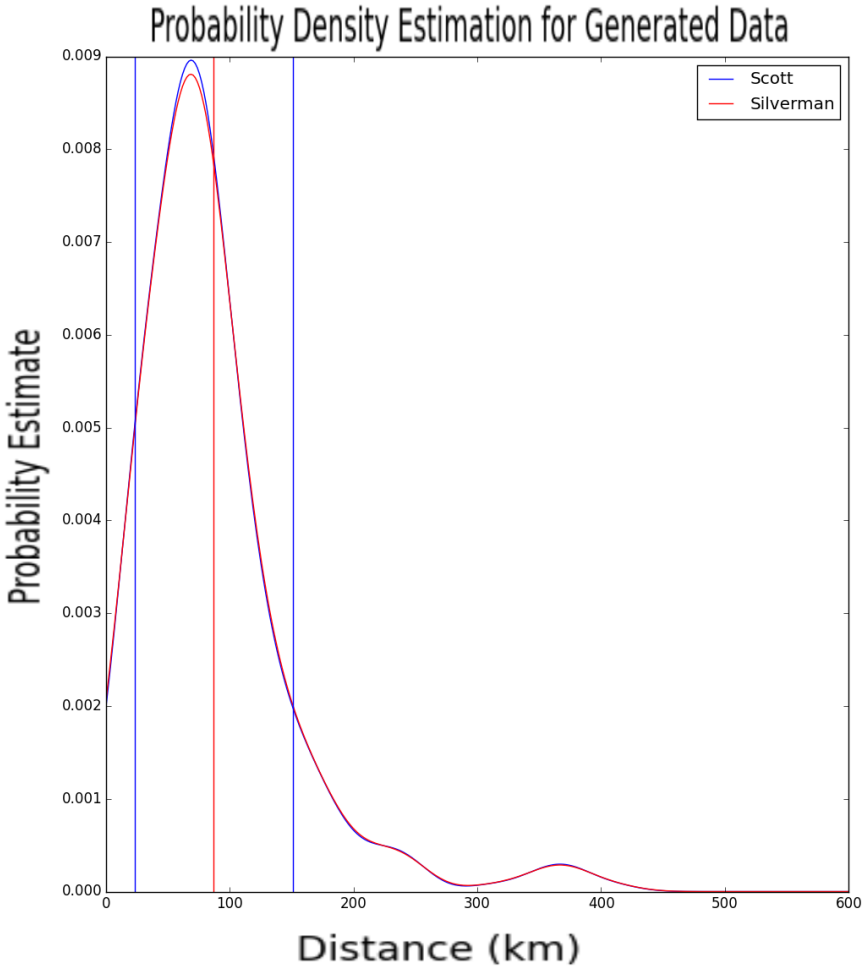

Figure 20: Probability estimates for the distance between any two randomly generated coordinates. Mean separation is shown as the red vertical line and the standard deviation is shown as the blue vertical lines. Probabilities calculated using both the Scott and Silverman smoothing estimations are shown.

No clusters containing more than 3 data points were found with separations of less than 60km (figure 15). This is important as the more data within a cluster and the smaller the separation of points in that cluster the stronger the evidence of grouping within the data is. The lack of any degree of clustering on the scale of geological features (such as Aristarchus crater at 40km diameter) suggests that there are no localised effects influencing the impacts catalogue.

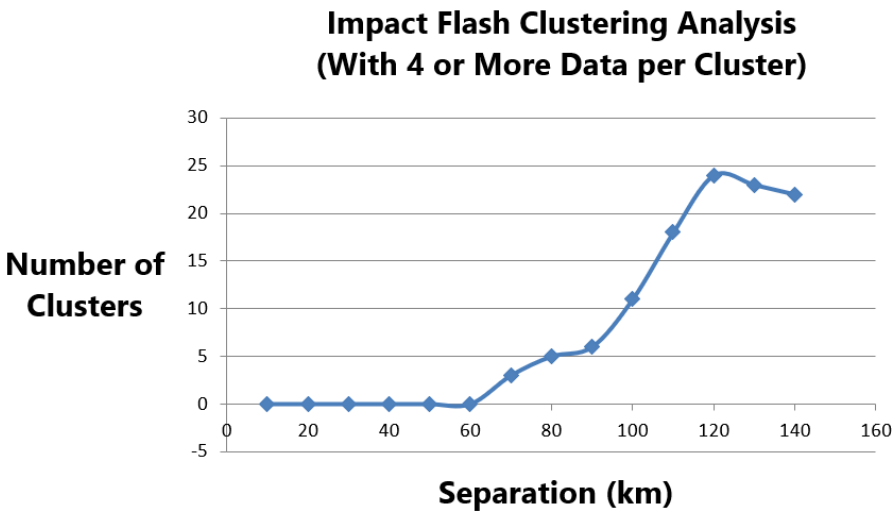

Figure 21: Number of clusters detected in the Marshall Space Flight Center catalogue dataset that contain more than 3 data. There are no clusters smaller than 60km.

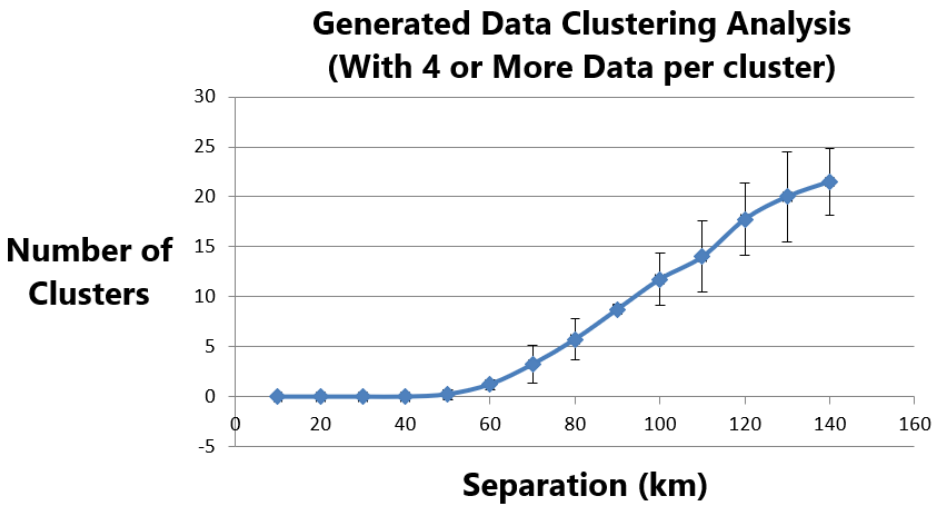

Figure 22: Number of clusters detected in the randomly generated dataset that contain more than 3 data. There are no clusters smaller than 60km.

4.6 Discussion

This analysis expected the signal of the Zito effect in the catalogued data to be an increase in probability of a close separation of impacts, resulting from local geographical variations such as a heavily bouldered areas and exposed rock faces in crater walls that may be struck by micrometeorites not large enough to produce their own impact flash or fracture under thermal stresses. This signal is completely missing from the data. The Zito effect is therefore a rare phenomenon or the light produced by the effect, which Zito demonstrated should be bright enough to be visible from Earth, is obscured. This obscuring of light would be especially prevalent further from the equator where light emanating from a fracture would not be directed at Earth or in boulders where the fracture may also be hidden from line of sight. The NASA database of impact flashes is unaffected by the effects proposed by Zito and also from any other localised flash producing effects that may be present on the lunar surface and can safely assumed to be an accurate catalogue of meteoric impacts.

5 Conclusions

The first study in this thesis aimed to use the X-ray spectrometer, C1XS, as a particle detector as previously outlined by Narendranath[14], to measure the width of the Geotail. The analysis compared data from C1XS with data generated by the OpenGGCM magnetohydrodynamic model running with historical solar wind data. Both datasets agreed on the position of the magnetopause to within a few hours of Chandrayaan-1's orbit during the April transit of the Geotail, when C1XS's data was clearest and most apparent, and whenever C1XS had significant data recorded it was in agreement with the MHD model to within 24 hours. This result is in agreement with the ARTEMIS satellite's measurements and suggests that future X-ray spectrometers using SCDs could be used to monitor magnetospheres as they transit through them.

The second study in this thesis examined Crotts' theory of lunar outgassing being responsible for the production of transient lunar phenomena. His papers suggest a correlation between the borders of lunar maria and TLP reports, where he expects the most outgassing to occur[22][23]. The analysis in this thesis created a digital representation of the mare borders using the Python programming language comprising of thousands of coordinates, and then recorded the closest point on the borders to each reported TLP in a catalogue compiled by Cook, for TLP reports of 5 weights sorted by robustness and reliability of the report, with observational nulls, and with randomly generated artificial reports. No correlation was found when only taking the most reliable reports into account, and further including the Aristarchus Plateau as highland terrain causes a large correlation due to the sheer number of TLP reported at Aristarchus crater, suggesting the

correlation is not with the borders but rather with specific features.

The final study in this thesis aimed to identify or constrain the effect proposed by Zito[45] as a possible explanation of TLP. Zito had calculated that light given off by gases excited by a piezoelectric effect from fracturing or cracking rocks on the lunar surface could be viewed from Earth. These flashes would have a similar duration and intensity to meteoric impact flashes and so the Marshall Space Flight Center impact flash catalogue was analysed to search for clustering of the data. Such a localised effect would not be expected in sporadic impact flashes, but could be explained by environmental features such as exposed crater walls or bouldered areas. The data produced no evidence of any localised effects, suggesting that the Zito effect is either a rarely seen phenomenon or that the light produced during the effect is obscured from view of an Earth observer. Future studies of the Zito effect should therefore focus on fainter flashes that may represent smaller or partially obscured flashes, and their distribution among particular features where other TLP effects are not expected, such as in heavily bouldered regions of the Moon.

References

[1] The European Space Agency, SMART-1. *www.esa.int/Enabling_Support/Operations/SMART-1*, www.ESA.int, 7^{th} November 2020.

[2] M Grande *et al. The D-CIXS X-ray mapping spectrometer on SMART-1*, Planetary and Space Science, Vol. 51, Issue 6, p427-433. 2003.

[3] B.G Lowe *et al. The Swept Charge Device, a Novel CCD-based EDX Detector: First Results*, Nuclear Instruments and Methods in Physics Research Section A: Accelerators, Spectrometers, Detectors and Associated Equipment, Vol. 458, Issues 1-2, p568-579. 2001.

[4] S Narendranath *et al. Lunar X-ray fluorescence observations by the Chandrayaan-1 X-ray Spectrometer (C1XS): Results from the nearside southern highlands*, Icarus, Vol. 214, Issue 1, p53-66. 2011.

[5] C J Howe *et al. Chandrayaan-1 X-ray Spectrometer (C1XS)-Instrument design and technical details*, Planetary and Space Science, Vol. 57, Issue 7, p735-743. 2009.

[6] J N Goswami, M Annadurai. *Chandrayaan-1 Mission to the Moon*, Acta Astronautica, Vol. 63, Issues 11-12, p1215-1220. 2008.

[7] M Grande *et al. The C1XS X-ray Spectrometer on Chandrayaan-1*, Planetary and Space Science, Vol. 57, Issue 7, p717-724. 2009.

[8] S Z Weider *et al. The Chandrayaan-1 X-ray Spectrometer: First Results*, Planetary and Space Science, Vol. 60, Issue 1, p217-228. 2012.

[9] A R Foster *et al. AtomDB 2.0: Updated Atomic Data for X-ray Astrophysics*, www.Atomdb.org 7^{th} November 2020.

[10] Kay *et al. The soft X-ray characteristics of solar flares, both with and without associated CMEs*, Astronomy and Astrophysics, Vol. 400, Issue 2, p779-784. 2003.

[11] P.S Athiray *et al. C1XS results - First measurement of enhanced sodium on the lunar surface*, Planetary and Space Science, Vol. 104, Part B, p279-287. 2014.

[12] T Okada *et al. X-Ray Fluorescence Spectrometer (XRS)on Kaguya: Current Status and Results*, 40th Lunar and Planetary Science Conference, Abstract #1897. 2009.

[13] P.S Athiray *et al. Experimental Validation of XRF Inversion Code for Chandrayaan-1*, Planetary and Space Science, Vol. 89, p183-187. 2013.

[14] S Narendranath *et al Observations of the Geotail While in Lunar Orbit by the Chandrayaan-1 X-ray Spectrometer (C1XS)*, 45th Lunar and Planetary Science Conference, Abstract #2199. 2014.

[15] S Agostinelli *et al. GEANT4 - A Simulation Toolkit*, Nuclear Instruments and Methods in Physics Research Section A: Accelerators, Spectrometers, Detectors and Associated Equipment, Vol. 506, Issue 3, p250-303. 2003.

[16] V Radhakrishna *et al. The Chandrayaan-2 Large Area Soft X-Ray Spectrometer(CLASS)*, 42nd Lunar and Planetary Science Conference. 2011.

[17] J N Goswami and M Annadurai. *Chandrayaan-2 Mission*, 42nd Lunar and Planetary Science Conference, Abstract #2042. 2011.

[18] K.E Chilton *Transient Lunar Phenomena*, Journal of the Royal Astronomical Society of Canada, Vol. 63, p203-205. 1968.

[19] J Burley, B.M Middlehurst *Apparent Lunar Activity: Historical Review*, Proceedings of the National Academy of Sciences, Vol. 55, Num. 5, p1007-1011. 1966.

[20] S Clarke *Now You See It*, Astronomy Now, Feb 2001, p62-63. 2001.

[21] A.P.S Crotts *Transient Lunar Phenomena: Regularity and Reality*, The Astrophysical Journal, Vol. 697, Num. 1, p1-15. 2009.

[22] A.P.S Crotts *Lunar Outgassing, Transient Phenomena, and the Return to the Moon. I. Existing Data*, The Astrophysical Journal, Vol. 687, Num. 1, p692-705. 2008.

[23] A.P.S Crotts, C Hummels *Lunar Outgassing, Transient Phenomena, and the Return to the Moon. II. Predictions and Tests for Outgassing/Regolith Interactions*, The Astrophysical Journal, Vol. 707, Num. 2, p1506-1523. 2009.

[24] R R Hodges and J H Hoffman. *Implications of Atmospheric ^{40}Ar Escape on the Interior Structure of the Moon*, 6th Lunar Science Conference. 1975.

[25] G F J Garlick, G A Steigmann and W E Lamb. *Effect of Fluidization on the Polarization of Reflected Light from Lunar dust Layers*, Nature Physical Science, Vol. 238, p13-14. 1972.

[26] G.F.J Garlick *Lunar Surface Movements - The Evidence and the Causes*, Philosophical Transactions of the Toyal Society of London, Series A, Mathematical and Physical Sciences, Vol. 285, Num. 1327, p325-329. 1977.

[27] W S Cameron. *Comparative Analyses of Observations of Lunar Transient Phenomena* Icarus, Vol. 16, Issue 2, p339-387. 1972.

[28] G.F.J Garlick *et al. An Explanation of Transient Lunar Phenomena from Studies of Static and Fluidised Lunar Dust Layers*, Proceedings of the Third Lunar Science Conference, Vol. 3, Lunar and Planetary Science Institute, p286-287. 1972.

[29] W.N Houston *et al. Downslope Movement of Lunar Soil and Rock Caused by Meteoroid Impact*, Proceedings of the Fourth Lunar Science Conference, Vol. 3, p2425-2435. 1973.

[30] L.A Taylor, Y Liu and A Zhang *Shape and Size Relationship of Several Lunar Dusts: Preliminary Results*, 40th Lunar and Planetary Science Conference, Abstract #2106. 2009.

[31] Y.J Pendleton *et al Dust Analysis at the Moon*, NASA presentation. *www.lpi.usra.edu/meetings/LEA/presentations/thurs_am/5_Pendleton_Dust_Analysis_at_the_moon.pdf*, www.lpi.usra.edu, 2007.

[32] J E McCoy and D R Criswell. *Evidence for a High Altitude Distribution of Lunar Dust*, Proceedings of the 5th Lunar Science Conference, Vol. 3, Pergamon Press, Inc., p2991-3005. 1974.

[33] T.J Stubbs *et al A Dynamic Fountain Model for Lunar Dust*, Advances in Space Research, Vol. 37, Issue 1, p59-66. 2005.

[34] M Horanyi *et al A Permanent Asymmetric Dust Cloud Around the Moon*, Nature, Vol. 552, p324-326. 2015.

[35] D G Sibeck and R Q Lin. *Size and Shape of the Distant Magnetotail*, Journal of Geophysical Research: Space Physics, Vol. 119, Issue 2. 2013.

[36] J Raeder and T Fuller-Rowell *OpenGGCM*, ccmc.gsfc.nasa.gov 20^{th} December 2020

[37] I G Akay *et al. Magnetotail Shape At Lunar Distances: ARTEMIS Observations*, 6th International Conference on Recent Advances in Space Technologies (RAST). 2013.

[38] W Herschel. *An Account Of Three Volcanoes In The Moon*, Philosophical Transactions of the Royal Society of London, Vol. 77, p229-232. 1787.

[39] L Wilson and J W Head. *Eruption Of Magmatic Foams On The Moon: Formation In The Waning Stages Of Dike Emplacement Events As An Explanation Of "Irregular Mare Patches"*, Journal of Volcanology and Geothermal Research, Vol. 335, p113-127. 2017.

[40] W S Cameron. *Lunar Transient Phenomena Catalog*, NSSDC 78-03. 1978.

[41] J J Rennilson and D R Criswell *Surveyor Observations of Lunar Horizon Glow* The Moon, Vol. 10, Issue 2, p121-142. 1974.

[42] E S Holden *Regarding Sir William Herschel's Observation Of Volcanoes In The Moon*, The Observatory, Vol. 11, p334-335. 1888

[43] T J Stubbs, R R Vondrak and W M Farrell *A Dynamic Fountain Model For Dust In The Lunar Exosphere*, Workshop on Dust in Planetary Systems (ESA SP-643), p185-189. 2007.

[44] J R Szalay and M Horányi *The Search For Electrostatically Lofted Grains Above The Moon With The Lunar Dust Experiment*, Geophysical Research Letters, Vol. 42, Issue 13, p5141-5146. 2015.

[45] R R Zito. *A New Mechanism for Lunar Transient Phenomena*, Icarus, Vol. 82, p419-422. 1989.

[46] J Harbaugh and B Dunbar.
www.nasa.gov/centers/marshall/overview/about.html,
www.NASA.gov, 2^{nd} January 2021.

[47] L Mohon and B Dunbar.
www.nasa.gov/centers/marshall/news/lunar/overview.html,
www.NASA.gov, 4^{th} August 2017.

[48] C Sweeney, D Thorpe and A Cook. *The Spatial Distribution of Lunar Impact Flashes*, EPSC Abstracts, Vol. 12, Abstract #1077. 2018.

[49] M C Jones *et al. A Brief Survey of Bandwidth Selection for Density Estimation*, Journal of the American Statistical Association, Vol. 91, Num. 433, p401-407. 1996.